DTU Library

Oxygen Exchange and Transport in $(La_{0.6}Sr_{0.4})_{0.98}FeO_{3-d}$ – $Ce_{0.9}Gd_{0.1}O_{1.95}$ Dual-Phase Composites

Ovtar, Simona; Søgaard, Martin; Norrman, Kion; Hendriksen, Peter Vang

Oxygen Exchange and Transport in $(La_{0.6}Sr_{0.4})_{0.98}FeO_{3-d}$ − $Ce_{0.9}Gd_{0.1}O_{1.95}$ Dual-Phase Composites

Simona Ovtar, [z] Martin Søgaard,[a] Kion Norrman, and Peter Vang Hendriksen*

Department of Energy Conversion and Storage, Technical University of Denmark, Risø Campus, 4000 Roskilde, Denmark

The chemical diffusion coefficient and the effective surface exchange coefficient (k_{ex}) of dual-phase $(La_{0.6}Sr_{0.4})_{0.98}FeO_{3-d}$ (LSF) − $Ce_{0.9}Gd_{0.1}O_{1.95}$ (CGO) composites containing between 30 and 70 vol.% of CGO were determined by electrical conductivity relaxation (ECR) at high oxygen partial pressures ($10^{-3} < pO_2 < 1$ atm) and at temperatures between 600°C and 900°C. The surface impurity segregation was detected by TOF-SIMS analysis. A large enhancement of k_{ex} was observed with increasing CGO fraction in the composite. k_{ex} was increased from 3.51×10^{-5} cm/s for a pure LSF to 1.86×10^{-4} cm/s for a 70 vol.% of CGO in the composite at 750°C for a pO_2 change from 0.2 to 1.0 atm. The experiments demonstrate that the k_{ex} is enhanced due to a synergistic effect between the two phases, and suggest a direct involvement of CGO phase in the oxygen surface exchange reaction. Possible mechanisms that could account for the synergy are the oxygen exchange process occurs also on the CGO surface, for example a spillover of absorbed oxygen ions from the LSF surface to the CGO surface or/and scavenging of impurities from one phase to another, thereby improving the oxygen exchange properties of the cleaned phase.

Perovskites within the $(La,Sr)(Fe,Co)O_3$ class of materials can potentially find application as catalysts, electrode materials in solid oxide fuel cells (SOFC) or solid oxide electrolysis cells (SOEC), in gas sensors and in oxygen transport membranes.[1–4] Both end members of the class; the iron free one (strontium doped lanthanum cobaltate)[5,6] as well as the cobalt free one (strontium doped lanthanum ferrite)[7–12] have been intensively studied. A large focus has also been on the specific composition $La_{0.6}Sr_{0.4}Co_{0.2}Fe_{0.8}O_{3-d}$ [4,13–15] (LSCF), which is especially promising for SOFC/SOEC applications due to a good compromise between oxygen transport properties and thermomechanical properties.

For the cobalt free perovskite of before mentioned class a partial substitution of La^{3+} with Sr^{2+} enhances strongly both the electronic and ionic conductivity. A 40 atom% Sr-substitution leads to an ionic conductivity of 0.014 S/cm[11] and electronic conductivity of 283 S/cm[8] at 800°C in air. $La_{0.6}Sr_{0.4}FeO_{3-\delta}$ is thus a mixed ionic electronic conductor (MIEC). The total conductivity of the strontium doped lanthanum ferrite depends on the oxygen non-stoichiometry and is function of the oxygen partial pressure (pO_2) in the surrounding atmosphere and temperature. In general, the ionic conductivity increases with decreasing pO_2 and the electronic conductivity is above a pO_2 of 10^{-12} atm predominantly p-type and below 10^{-12} atm n-type.[8] The change of electronic conductivity (σ_{el}) with pO_2 follows the relation $\sigma_{el} \propto pO_2^{-1/4}$ at low pO_2 and $\sigma_{el} \propto pO_2^{1/4}$ at high pO_2 as expected from a simple defect model considering $Sr_{La}^{\bullet}$, $Fe_{Fe}^{\bullet}$, $Fe_{Fe}^{'}$ and $V_o^{\bullet\bullet}$ to be the predominant defects.[8]

The oxygen transport through MIEC materials is determined by the rate of the oxygen exchange over the gas solid interface and the diffusivity of oxide ions and electrons (or holes) in the bulk. The oxygen surface exchange coefficient (k_O) and the oxygen diffusion coefficient (D_O) are commonly quantified using oxygen isotope diffusion profiles obtained from secondary ions mass spectrometry (SIMS),[16] and from electrical conductivity relaxation (ECR)[11] experiments (where one measures chemical diffusion coefficient (D_{chem}) and effective surface exchange coefficient (k_{ex}), and more recently from Pulsed Isotope Exchange (PIE), using powder samples.[17]

The oxygen exchange reaction is in general a complex process that involves several reaction steps including O_2 adsorption on the surface, dissociation and charge transfer (all together hereinafter referred to as surface exchange) and finally incorporation of ionized species into crystal lattice (oxygen incorporation). In the literature comprehensive discussions about the possible mechanisms of oxygen exchange in oxygen deficient MEIC perovskites can be found.[7,9,10,12,18–22] During the process, several different oxygen species may occur as intermediates [$O_{2,ads}$, $O_{2,ads}^{-}$, $O_{2,ads}^{2-}$, O_{ads}^{-}] and for different perovskite materials different species may be involved in the rate determining step (*rds*). The variation of the k_{ex} with pO_2 can in some cases elucidate the *rds* of the overall oxygen exchange reaction. Different mechanisms of the oxygen exchange on perovskite materials have been discussed.[7,10,18,19,23,24] Merkle et al.[18] proposed for the experimental findings on Fe doped $SrTiO_3$ that the *rds* contains the dissociation of molecular oxygen species with or without electron transfer. ten Elshof et al.[10] proposed on the basis of pO_2 dependencies of k_O for LSF that the *rds* involves at least an oxygen molecule and a vacant oxygen site at the surface and that for LSCF[25] the *rds* involves molecular oxygen. Mosleh et al.[7] for experimental studies carried out on LSF thin films prepared with PLD point to that the first step is the oxygen adsorption and the rate limiting step is dissociation of the oxygen species involving two oxygen vacancies.[7] However, for the studies on thin films the activation energy and total reaction rate were different from what is observed on bulk LSF and composite electrodes and hence the mechanism deduced from these thin films[7] does not necessarily represent the situation here. Deviations in behavior between studies on thin films and bulk/composite samples can be due to differences in stress state, structure and most importantly surface composition.

For most MIECs the concentration of oxygen vacancies and electron holes strongly depends on temperature and pO_2, which results in a variety of reported pO_2 dependencies of k_{ex} for this class of materials.[9–11,26,27] Additionally, Fleig et al.[23] reported that the presence of ionized oxygen species on the surface especially at high pO_2 strongly reduces the dependence of k_{ex} on pO_2 (through electrostatic effects) and hinder distinction between different possible surface exchange mechanisms and their rate determining steps.

The oxygen transport in oxygen deficient perovskites is generally considered to occur via a vacancy hopping mechanism and the rate of the transport is related to the vacancy concentration and mobility. A strong correlation between D_o and k_O for many of oxygen deficient MEIC perovskites has been reported.[20,22,27–30] From this it was proposed that the same mechanisms are operative for the whole class of materials and that oxygen vacancies play a major role in the oxygen exchange of these materials. Furthermore, high mobility and high concentration of oxygen vacancies are criteria for fast oxygen exchange kinetics, as highlighting by Wang et al.[22] The presence of phases with higher ionic conductivity (higher concentration of highly mobile vacancies) in proximity to a MIEC perovskite could be speculated to

*Electrochemical Society Member.
aPresent address: Meneta Group, DK-5270 Odense N, Denmark.
zE-mail: simov@dtu.dk; simona.ovtar@gmail.com

locally improve the oxygen exchange rate. This is certainly the case for triple-phase boundary-type composite electrodes of an electro-catalyst like strontium doped lanthanum manganite (LSM) and an ionic conductor like ceria or zirconia.[31,32] There, the electrode reaction relies on the incorporation of oxygen in to the ionic conductor in the proximity of the electro-catalyst.[31–36] The reaction zone in these composites is limited to narrow zone at the triple-phase boundary (TPB) and the overall oxygen exchange increases with the increase of the TPB length.[31,33–35]

Studies on dense MIEC dual-phase composites like $La_{0.6}Sr_{0.4}Co_{0.2}Fe_{0.8}O_{3-d} - Ce_{0.8}Sm_{0.2}O_{2-d}$,[37] $Sr_2Fe_{1.5}Mo_{0.5}O_6 - Ce_{0.8}Sm_{0.2}O_{2-d}$,[21,38] $La_{0.8}Ca_{0.2}CoO_3 - Ce_{0.8}Sm_{0.2}O_{2-d}$[39] or $La_{0.6}Sr_{0.4}Co_{0.8}Fe_{0.2}O_{3-d} - Ce_{0.9}Gd_{0.1}O_{2-d}$[40] has demonstrated an increased oxygen exchange rate by the addition of a good ionic conductor, $Ce_{0.8}Sm_{0.2}O_{2-d}$ (CSO) or $Ce_{0.9}Gd_{0.1}O_{2-d}$ (CGO), compared to the bare MIEC. Recently, it was also shown that for dual-phase composites of $Sr_2Fe_{1.5}Mo_{0.5}O_6 - CSO$, where the rate limiting process for the oxygen transport at 750°C and high pO_2 is the oxygen exchange, the effective surface exchange rate can be increased by increasing the volume fraction of CSO, which was ascribed to an TPB length increase.[21]

Even for single phases like $La_{0.6}Sr_{0.4}FeO_{3-d}$,[41] $La_{0.6}Sr_{0.4}Co_{0.8}Fe_{0.2}O_{3-d}$,[15,42] $Sr_2Fe_{1.5}Mo_{0.5}O_6$[38] that were surface coated with CSO or CGO a similar behavior was observed. The surface exchange rate of the coated surfaces compared to the bare one was increased by a factor of 10 to 100. Hong et al.[15] suggested that the increase originates from the reaction occurring at the TPB and that the surface exchange rate must be substantially higher than that on the "pure" LSCF surface.

The aim of this study is to characterize the oxygen transport properties of a dual-phase composite system as a function of temperature and to elucidate the origin of the enhancement of the oxygen surface exchange reaction occurring with increasing the amount of the ionic conductor. The study contains two parts. In the first part, the oxygen transport properties of samples with different volume fractions of $(La_{0.6}Sr_{0.4})_{0.98}FeO_{3-\delta}$ (LSF) and $Ce_{0.9}Gd_{0.1}O_{1.95}$ (CGO) are discussed based on ECR measurements. In the second part, a sample with 70 vol.% of CGO and 30 vol.% of LSF and with adjusted microstructure was investigated by of time-of-flight secondary ion mass spectrometry (TOF-SIMS) to investigate surface impurities segregation on the dual-phase composite.

Possible Mechanisms of Oxygen Exchange for Dual Phase Composites

Oxygen exchange on dual-phase composites have been discussed by several groups as mentioned in the introduction. Different involvements of the two phases in the oxygen exchange were proposed. The predicted conductivity relaxation curve after a sudden step change of pO_2 for dual phase composites for different assumptions regarding the active surface is illustrated in Figure 1. The following assumptions are made; i) random distribution of phases, ii) oxygen exchange is much slower than bulk transport in the material, iii) the oxygen concentration changes only in the P1 phase, and iv) the surface area fraction (f_{S1}) and volume fraction (f_{V1}) of the P1 phase are equal. In this case, the normalized conductivity change can be described by Eq. 1;

$$f(t) = \frac{\sigma_\infty - \sigma(t)}{\sigma_\infty - \sigma(t_0)} = exp\left(-t \cdot \frac{S_1}{V_1} \cdot k_1\right) \quad [1]$$

Where σ_∞ is the conductivity at the new equilibrium, $\sigma(t)$ is the conductivity at time t during the relaxation and $\sigma(t_0)$ is the conductivity before the step change in pO_2. S_1 is the surface area of the P1 phase, V_1 is the volume of P1, t is time and k_1 is the efficient surface exchange coefficient of the P1 phase. This simplification gives a direct illustration of the influence of surface area and volume of the phases, where the oxygen content varies, on the shape of a relaxation curve. In dual-phase composites where only one phase (P1) changes oxygen concentration (like LSF in the here studied case), and in a case that this phase is also the only one active for the oxygen exchange, the conductivity relaxation curve will for a constant S_1/V_1 ratio not be
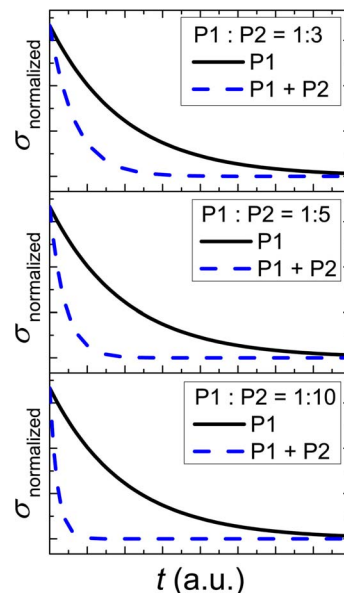
Figure 1. Schematic presentation of a conductivity relaxation curve for a surface controlled process after a step change of pO_2 for composites (P1+P2; P1 is a MIEC and P2 is a ionic conductor, which nonstoichiometric is unchanged) with different phase ratios (P1: P2); with only P1 involved in the surface exchange (solid line) and with both P1 and P2 involved in the surface exchange (dashed line).

affected by the change in the phase ratio (P1: P2), as illustrated in Figure 1. Contrary, for equal involvement of both phases (P1 and P2) in the oxygen exchange, and if only the P1 phase can take up/release oxygen, increasing the amount of the P2 phase will result in shorter relaxation times. In this case Eq. 2 needs to be used to fit the model to the experimental relaxation data.

$$f(t) = \exp\left(-t \cdot \frac{S}{V_1} \cdot (f_{S1}k_1 + f_{S2}k_2)\right)$$
$$= \exp\left(-t \cdot \frac{S}{V} \cdot \left(k_1 + \frac{f_{S2}}{1 - f_{S2}}k_2\right)\right) \quad [2]$$

Here k_1 and k_2 represent the surface exchange coefficients on the P1 and P2 phases, respectively. f_{S1} and f_{S2} are the surface area fraction of the P1 phase and the P2 phase, for which holds that $f_{S1} + f_{S2} = 1$. The right part of the equation is derived by assumption that $f_{S1} = f_{V1}$ and $f_{S2} = f_{V2}$. S represents the total surface of the sample and V represents the total volume of the sample.

Besides, as described above, considering the general involvement of the two phases in the oxygen exchange, one has to account for different possibilities where the surface exchange and oxygen incorporation will take place. Different steps and possible routes of oxygen surface exchange reaction in the composite are illustrated in Figure 2. In the following specific limiting cases that can be correlated to the findings reported in the here presented study will be considered (in the sections Fast oxygen exchange on LSF – Involvement of CGO in the oxygen surface exchange reaction), with the aim to describe the dependence of the effective surface exchange coefficient on bulk properties of the composite.

Fast oxygen exchange on LSF.—The effective surface exchange coefficient can for the dual-phase LSF-CGO composite be described by:

$$k_{ex(sample)} = k_{ex(LSF)} + \frac{f_{S2}}{1 - f_{S2}}k_{ex(CGO)} \quad [3]$$

Where, f_{S2} represents the surface area fraction of the CGO phase in the composite, $k_{ex\ (sample)}$ is the effective surface exchange coefficient
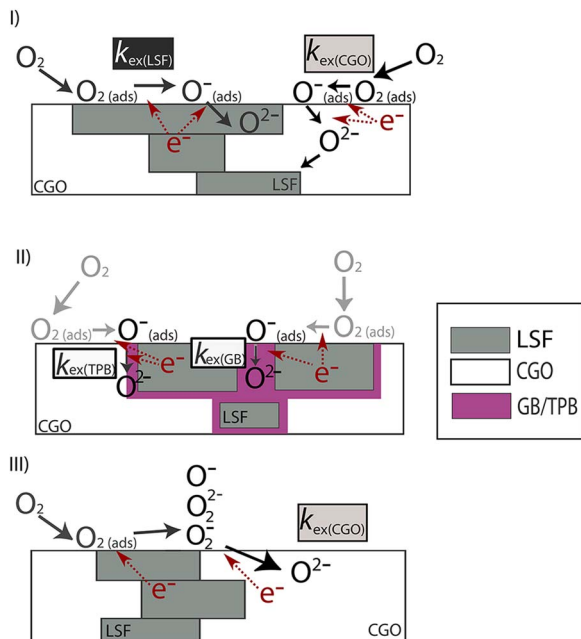
Figure 2. Schematic presentation of possible routes of oxygen exchange with different locations of the oxygen incorporation; I) independently occurring on LSF and CGO, II) primarily occurring on grain boundaries, III) occurring on LSF and CGO, with spillover mechanism.

of the composite, $k_{ex(LSF)}$ is the surface exchange coefficient of the LSF phase and $k_{ex(CGO)}$ is the surface exchange coefficient of the CGO phase.

Several studies of k_{ex} on LSF by conductivity relaxation are available in literature.[7,9,11,26] For CGO data is scarcer. Two different hypotheses can be postulated on base of the reported oxygen exchange properties of doped ceria; a) the CGO is inactive for oxygen surface exchange at high pO_2 (compared to LSF) and b) CGO surface is active for oxygen surface exchange.

a) In support of this, very low oxygen surface exchange coefficients (k_O) of CGO have been reported at various conditions.[43,44] The experimental investigations show that $k_{O(CGO)} = 1.1 \times 10^{-8}$ cm/s at 700°C[45] whereas exchange is a 1000 times faster on LSF; $k_{O(La_{0.8}Sr_{0.2}FeO_3)} = 4.0 \times 10^{-5}$ cm/s at 750°C,[46] as determined from [18]O isotope diffusion profiles. Thus, most of the oxygen reduction will occur at the LSF surface. If the two materials in the composite behave independently with respect to the oxygen exchange, the addition of a doped ceria (with constant oxygen stoichiometry) will increase the oxygen diffusion coefficient but the overall surface exchange coefficient will for a constant S_1/V_1 ratio remain constant.

b) Recently, relatively fast surface exchange (k_{ex}) has been reported on a similar system, $Ce_{0.85}Sm_{0.15}O_{2-x}$[47] measured by ECR, which hints that the doped ceria can be active for oxygen exchange also at a high pO_2. In this case, the both surfaces LSF and CGO can in principle be active for the oxygen surface exchange reaction as illustrated in Figure 2I. The addition of doped ceria will speed up not only oxygen diffusion but also oxygen exchange.

Fast oxygen exchange on grain boundaries.—In case that the *rds* involves a vacant oxygen site at the surface (for adsorption as proposed by ten Elshof et al.,[10] or for dissociation of oxygen molecules, as proposed by Mosleh et al.,[7] or for oxygen incorporation into the oxide crystal lattice) the increase of the oxygen vacancies mobility and their concentration should result in an increased k_{ex}. Grain boundaries could possibly be fast reduction and dissociation sites with a higher concentration of defects. The here studied composites have two

different types of grain boundaries; a single phase grain boundary (GB) and a dual-phase grain boundary (TPB).

For a GB in CSO (10^{-30} atm $< pO_2 < 10^{-18}$ atm) it has been reported that at low temperature the surface exchange rate depends on the grain size of the studied material. This is likely associated with the concentration of oxygen vacancies being significantly higher at the grain boundary than on the surface of CSO grains, while at ≥ 800°C the oxygen exchange was independent on grain size.[48] Contribution of gains and grain boundaries to the oxygen exchange and the oxygen diffusion in LSM thin films with controlled grain sizes ranging from 30 nm to 75 nm was reported by Navickas et al.[49] In that case, the grain boundary diffusion and the grain boundary surface exchange were approximately two to three orders of magnitude larger than those of the grains.

For a TPB in dual-phase $Sr_2Fe_{1.5}Mo_{0.5}O_6$−CSO composites it was from relaxation results suggested that more than 90% of the overall oxygen uptake occurs at the TPB, for a TPB length between 0.50×10^{-6} and 1.46×10^{-6} m^{-1}.[21] Similar conclusions were reached for a $La_{0.6}Sr_{0.4}Co_{0.2}Fe_{0.8}O_{3-d}$−CSO composite, where 70% of the oxygen uptake at 650−800°C was reported to occur at the TPB.[37] Inspired by these observations it is hypothesized that also for the here studied LSF-CGO composite the grain boundaries could act as zones of fast dissociation/incorporation. It would then be expected that k_{ex} will be enhanced by increasing the GB or/and TPB lengths. The effective surface exchange coefficient can for this case be written

$$k_{ex(sample)} = k_{ex(LSF)} + \frac{f_{LSF-GB}}{f_{V1}} k_{ex-LSF(GB)} + \frac{f_{CGO-GB}}{f_{V1}} k_{ex-CGO(GB)}$$

$$+ \frac{f_{TPB}}{f_{V1}} k_{ex(TPB)} \qquad [4]$$

The f_{i-GB} represents the surface area fraction of single phase grain boundaries (i = LSF or CGO), and f_{TPB} the surface area fraction of dual-phase boundaries. The $k_{ex-LSF(GB)}$ and $k_{ex-CGO(GB)}$ are the effective surface exchange coefficient on the single-phase grain boundaries and $k_{ex(TPB)}$ is the effective surface exchange coefficient on the dual-phase grain boundaries (as illustrated in Figure 2II).

Involvement of CGO in the oxygen surface exchange reaction.— Besides, the two previously presented limiting cases of exchange occurring independently on the LSF and CGO surfaces, or enhanced exchange at the GB/TPB a third possibility of synergy between the two phases is schematically illustrated in Figure 2III. Possibly the CGO surface could contribute by incorporating oxygen ions (O^-, O^{2-}, O_2^{2-}, O_2^-), which are formed on LSF and spilled over to the CGO surface,[40] i.e. the dissociation of ionized oxygen molecules, final ionization of O^- to O^{2-} ion and incorporation into the oxide crystal lattice occurs at the CGO surface. The final ionization (O^- to O^{2-}) in the mixed conductors is assumed to be fast,[22] therefore the low, but non-negligible electronic conductivity of CGO (8×10^{-4} S/cm at 900°C and 0.21 atm),[50] is speculated to be high enough that electron transfer can occur during the incorporation reaction at CGO. In this case the addition of better ionic conductor (CGO) will improve both the oxygen diffusion and the effective surface exchange rate, which can be described with Eq. 3.

Another synergistic effect was recently reported, namely that a transition metal perovskite in the vicinity of the CGO surface may act to remove impurities from the CGO surface. The oxygen exchange on the "cleaned" CGO surface appears to be very fast,[40] and possibly, in the older SIMS studies of single phase CGO the exchange reaction has been impeded by unintended impurities on CGO surface.

Experimental

Sample preparation.—CGO ($Ce_{0.9}Gd_{0.1}O_{1.95}$, Rhodia) and LSF (($La_{0.6}Sr_{0.4})_{0.98}FeO_3$, Kusaka, Japan) were mixed in the following volume % ratios CGO:LSF = 70:30 (CGO70), 50:50 (CGO50), 30:70 (CGO30). The powder mixtures and pure LSF were ball milled in ethanol using ZrO_2 balls for 24 h at 50 rpm (with volume ratio;

Table I. Overview of the samples key characteristics; sintering time, density of sample (%TD), conductivity, surface areas of the two phases and TPB length derived from image analysis of the micrographs.

Sample	$t_{(sintering)}$ [h]	Surface area LSF	Surface area CGO	% TD	Length of TPB [$\mu m/\mu m^2$]	Conductivity at 750°C in air [S/cm]
LSF	2	1	0	98.7	/	246
CGO30	2	0.69	0.31	99.7	2.8 ± 0.1	90
CGO50	2	0.46	0.54	96.9	2.7 ± 0.1	35
CGO70	2	0.26	0.74	99.3	2.1 ± 0.1	4.0
CGO70-3M	3	0.25	0.75	100.0	2.3 ± 0.1	4.6
LSF-1200+CGO	10	0.29	0.71	97.4	0.16 ± 0.03	0.2

1/4 powder, 1/4 ethanol and 1/2 of ZrO_2 balls). The slurries were dried and the mixtures of CGO and LSF powders and pure LSF were pressed uniaxially into rectangular bars with a pressure of 30 MPa. The bars were further compressed isostatically at 325 MPa and were subsequently sintered at 1300°C for 2 h. To increase the TPB length for the CGO:LSF = 70:30 composition the LSF and CGO powders were ball milled for 3 days (CGO70-3 M) which significantly reduced the particle size. Geometrical densities of all samples were larger than 95% of the theoretical density, as is listed in Table I. All surfaces of the bars were ground and polished with 1 μm diamond polishing agent to obtain bars with size of $2.5 \times 1.5 \times 20$ mm^3. After polishing, the bars were re-annealed in air at 1000°C for 12 h.

A sample (LSF-1200+CGO sample) with a microstructure adjusted to the spatial resolution of TOF-SIMS was prepared from the LSF powder that was pre-calcined at 1200°C for 3 h and the as-received CGO powder. The sample was sintered at 1300°C for 10 h to reach 97.4% of the theoretical density, polished and re-annealed at 1000°C.

Characterizations.—Phase purity of sintered and annealed bars before the relaxation measurements was determined using a BrukerD8 X-ray diffractometer with CuKα radiation ($\lambda = 1.5406$ Å). The microstructure of the re-annealed samples was investigated by scanning electron microscopy (SEM, SUPRA Zeiss). The length of the TPB (CGO-LSF-O$_2$) and the surface area of both phases were calculated from several SEM images per sample using an in-house developed software. The surface chemistry of the sample LSF-1200+CGO after the same exposure to high temperatures and different atmospheres (the same as the samples experience during the ECR measurements) was mapped using time-of-flight secondary ion mass spectrometry (TOF-SIMS IV from ION-TOF GmbH, Münster, Germany).

A four point DC method was used for conductivity measurements. Pt wires attached to both ends of the sample were used as current probes. A Pt past (64021015 Pt paste, Ferro GmbH, Germany) was painted at the far edges of the rectangular bar to improve the contact between the sample and the current probes. For voltage probes Pt wires of thickness 0.3 mm were mounted symmetrically around the middle of the sample with a distance of 5 mm from each other ($\sim$7 mm from the current probes). The electrical conductivity of the samples was measured as a voltage drop over a well-defined distance in the center of the samples when a current of 10 mA was applied. Two samples were placed in a quartz tube and were heated up to 900°C with ramp rate of 60°C/h in air. The samples were left for 8–12 h to stabilize at the temperature. Measurements were carried out at 900°C, 750°C and at 600°C with heating and cooling rates of 60°C/h. The total gas flow was kept constant at 12 l/h and was controlled using 4 mass flow controllers (Brooks). The oxygen partial pressure was changed by varying the flow rates of air, nitrogen and oxygen with an in-house constructed 4 way valve system. The gas mixture was released in the vicinity of the samples allowing the atmosphere in the tube to be changed in less than 10 s. The pO_2 was varied in the range from 1 to 0.01 atm with a typical step for reduction $pO_{2\,final}$ = 1/2* $pO_{2\,initial}$ and for oxidation $pO_{2\,final}$ = 2* $pO_{2\,initial}$. At 600°C larger steps in pO_2 change (from 1.0 atm to 0.2 atm and from 0.2 atm to 0.1 atm) were used, due to small conductivity change with pO_2. For the comparison the same pO_2 changes were additionally

also applied at other temperatures. pO_2 was monitored in the inlet and outlet gasses using an in-house constructed zirconia-based oxygen sensor. The analysis of data of the oxygen transport properties for pO_2 < 0.01 atm was done by taking gas concentration polarization into consideration, due to the uptake/release of oxygen from the sample.[51]

Fitting parameters.—ECR is a well-established method to determine the oxygen transport properties of MIECs.[10,11] ECR measures a change of the conductivity of a sample being subjected to a step change in the surrounding pO_2. At $t = 0$ the pO_2 is abruptly changed to a new value, which leads to a new equilibrium concentration of oxygen vacancies in the material. As the conductivity of the MIEC depends on the concentration of charge carriers via the electroneutrality condition the change of conductivity after a change in the pO_2 can, for well-defined geometries, be correlated to the oxygen transport properties of the material. By fitting the conductivity change using Fick's law of diffusion with appropriate boundary conditions, the values of k_{ex} and D_{chem} can be obtained. Assumptions used in the data analysis include: i) local electro-neutrality, ii) linear surface exchange kinetics, iii) a linear relationship between the conductivity and the oxygen vacancy concentration, iv) a constant value of D_{chem} and k_{ex} during the relaxation, and v) that for a two-dimensional system the oxide ion concentration is in local equilibrium in x and y direction. The two-dimensional diffusion problem with a first order surface reaction can be described using Eq. 5, which was used for fitting the normalized conductivity.[11]

$$f(t) = \frac{\sigma_\infty - \sigma(t)}{\sigma_\infty - \sigma(t_0)} = \sum_{n=1}^{\infty} \frac{2L_x^2 \exp\left(\frac{-\beta_{n,x}^2 D_{chem} t}{l_x^2}\right)}{\beta_{n,x}^2 \left(\beta_{n,x}^2 + L_x^2 + L_x\right)}$$

$$\sum_{n=1}^{\infty} \frac{2L_y^2 \exp\left(\frac{-\beta_{n,y}^2 D_{chem} t}{l_y^2}\right)}{\beta_{n,y}^2 \left(\beta_{n,y}^2 + L_y^2 + L_y\right)} \quad [5]$$

$$\beta_{n,x}^2 \tan \beta_{n,x}^2 = L_x \quad L_x = \frac{l_x k_{ex}}{D_{chem}}, \quad \beta_{n,y}^2 \tan \beta_{n,y}^2 = L_y \quad L_y = \frac{l_y k_{ex}}{D_{chem}}$$

$$[6]$$

$2l_x$ and $2l_y$ are the width and thickness of the sample. For accurate ECR results the sample dimensions should fulfill the criteria of $l_x \approx l_y << l_z$, where z is the direction of the electrical current and $2l_z$ the length of the sample. A two-dimensional solution of the diffusion problem is used in the fitting because the conductivity is measured over a short distance close to the center of a long rectangular bar. Details relating to the fitting can be found elsewhere.[52] The error bars shown in the later figures represent D_{chem} and k_{ex} values within the 5% of standard deviation from the best fit values. For the dual-phase LSF-CGO composites it was additionally assumed that i) the conductivity change after pO_2 step reflects only a change of oxygen concentration in LSF (since for the studied temperature and pO_2 range the oxygen stoichiometry of CGO is known to be virtually constant and the total conductivity is dominated by the electronic conductivity of the percolating LSF phase)[50] and ii) the phases are randomly distributed in the composite.

The measured D_{chem} was fitted with theoretically calculated D_{chem} from the effective vacancy diffusion coefficient of a dual-phase
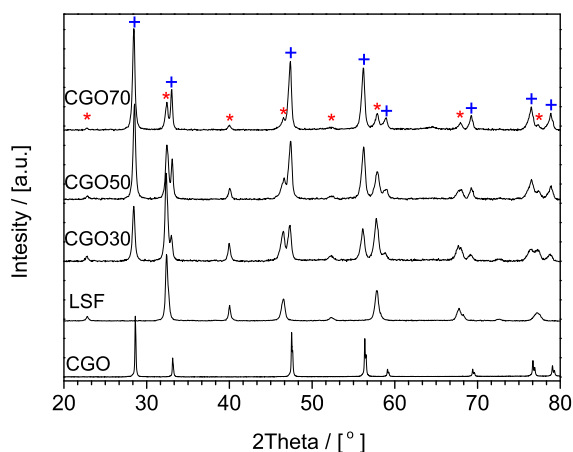
Figure 3. XRD patterns of sintered bars of pure LSF, LSF-CGO composites and CGO powder. (+) are the CGO peaks and (*) are the LSF peaks.

composite material ($\bar{D}_V$), which depends on the diffusion coefficients of both phases. Fundamental continuum assumption, where composite can be modeled as a weighted superposition of the phases that it is comprised of, with the following assumptions; i) random distribution of phases, ii) local equilibrium of oxygen vacancies in all planes parallel to the z-axis, iii) that electron processes do not limit the oxygen transport, and iv) that $\partial C_{v,IC}/\partial t = 0$, was used for calculating the $\bar{D}_V$ using Eq. 7.[53]

$$\bar{D}_V = \frac{\phi_{IC}}{\tau_{IC}} \frac{C_{v,IC}}{C_{v,MC}} D_{v,IC} + \frac{\phi_{MC}}{\tau_{MC}} D_{v,MC} \qquad [7]$$

Where ϕ_{IC} and ϕ_{MC} are the volume fractions, τ_{IC} and τ_{MC} are the tortuosities and $C_{v,IC}$ and $C_{v,MC}$ are concentrations of vacancies in the ionic conductor and the mixed conductor, respectively. $D_{v,IC}$ and $D_{v,MC}$ are the vacancy diffusion coefficients of the ionic conductor and mixed conductor, respectively. The vacancy diffusion coefficient of LSF ($D_{V,MC}$) was calculated from the measured D_{chem}[11] by knowing the vacancy thermodynamic enhancement factor (Γ_V) and the oxygen non-stoichiometry (δ). Γ_V and δ were calculated from thermodynamic data and equations reported in Mosleh et al.[7] and Søgaard et al.[11] The ionic conductivity of the CGO reported by Dalslet et al.[54] was used to calculate $C_{v,IC} \cdot D_{v,IC}$. D_{chem} of the composite was calculated from $\bar{D}_V$ assuming that only LSF changes oxygen stoichiometry in the studied pO_2 range and therefore only Γ_V of LSF was used. It should be noted that the tortuosities in the above equation are complex functions of the microstructure of the overall composite, but they also depend on the relative magnitude between the vacancy diffusion coefficients of the ionic and the mixed conductor.[53]

Results

Phase composition and microstructure.—The X-ray diffractograms of the pure LSF, the dual-phase LSF-CGO composites after sintering at 1300°C and of the CGO powder are shown in Figure 3. In the XRD patterns of the dual-phase composites only two phases can be observed, indicating that no new crystalline phases have formed. No peak shifts in the XRD patterns could be observed compared to the pure LSF and CGO powders, indicating that a cation diffusion between LSF and CGO is negligible.

Volume fraction variation.—In Figure 4 the SEM micrographs of the polished samples are shown. Figure 4A shows the microstructure of the thermally annealed pure LSF sample. The average grain size determined from image analysis was 2.0 ± 1.5 μm. The microstructures of the polished CGO30, CGO50 and CGO70 composite are illustrated in Figures 4B, 4C, 4D, respectively. The microstructures were

obtained using back scattered electrons, to highlight the variation in phases' fractions. The bright phase is CGO with the average grain size of 0.55 ± 0.22 μm and the dark phase is LSF with the average grain size of 0.50 ± 0.26 μm. The surface areas of LSF and CGO derived from the SEM micrographs for the composites are listed in Table I. As expected, the measured surface area ratios are similar to the volume fraction used for preparation of the composites. The TPB length, also derived from SEM micrographs, decreases with the increasing CGO volume fraction. There is however no clear maximum at the expected 50 vol.% LSF: 50 vol.% CGO composite. The variation from CGO30 to CGO50 and CGO70 seems to be more controlled by small unintended differences in the grain sizes of the CGO and LSF grains and difference in agglomeration of each phase than by the volume ratio (Table I).

Morphology variation.—With a longer milling time of the powders the final grain size of the sintered composite was slightly decreased to 0.45 ± 0.22 μm for the CGO grains and to 0.35 ± 0.17 μm for the LSF grains (Figure 5A), compared to the grain size of the sintered as-received powders (Volume fraction variation section). The TPB length of the CGO70-3 M sample was slightly increased (Table I).

For the composite with the pre-calcined LSF powder the average grain sizes were 0.9 ± 0.6 μm and 1.1 ± 0.8 μm for CGO and LSF, respectively (Figure 5B) and were approx. twice larger than for the composites prepared from the as-received powders. The LSF-1200+CGO sample consists of large multi-grain LSF islands in range of 10's μm in a CGO matrix.

Electrical conductivity.—The samples' total conductivity includes both an electronic and an ionic contribution. However, for pure LSF and the LSF-CGO composites studied here the ionic contribution to the total conductivity is small ($\sigma_i < \sigma_{el}/100$) and the major contribution to the measured total conductivity comes from electronic conductivity of LSF. The conductivity of the pure LSF and the LSF-CGO composites increases with temperature, goes through a broad maximum and then decreases. Below 600°C the activation energy of the conductivity of LSF as well as the composites is in the range of 5.8 to 7.7 kJ/mol. The temperature dependence of the LSF conductivity found in the present study as well as the activation energies are in good agreement with values that can be found in the literature.[7,8]

The total conductivity of the composites is lower than that of the pure LSF, due to much lower total conductivity of CGO (Table I). The total conductivity in air at 750°C for the CGO70 is only 4.0 S/cm compared to 250 S/cm for the pure LSF. However, even at 70 vol.% of CGO in the composite the microstructure still enables percolation of the electronically conductive phase[55] and the total conductivity is around 40 times higher than for the pure CGO.[50] The microstructure of the composites also strongly influences the total conductivity, as it is evident from the 70 vol. % of CGO composites in Table I. Formation of larger LSF islands in the CGO matrix (LSF-1200+CGO sample) strongly reduces the electrical conductivity, due to a decreased fraction of the percolating LSF grains.

The total conductivity of LSF decreases with decreasing pO_2 as a consequence of an increased concentration of oxygen vacancies and the associated reduction of the electron hole concentration. The pO_2 dependence of the total conductivity of LSF increases with temperature and for the highest temperature (900°C) in Figure 6A the slope approaches $\frac{1}{4}$, which is expected when the material is becoming gradually more non-stoichiometric.[7,8,11,12,51] At lower temperature, the pO_2 dependence of the total conductivity is smaller (see Figure 6C). As the temperature decreases, the concentration of oxygen vacancies in LSF decreases.[11] Consequently, at low temperature the dopant (Sr^{2+}) is mostly electrically compensated, which results in the weaker pO_2 dependence. The observed pO_2 dependence of the total conductivity of the composites is the same as that observed for the pure LSF sample (Figure 6), further illustrating that the conductivity of the composites is completely dominated by the electronic conductivity of LSF.
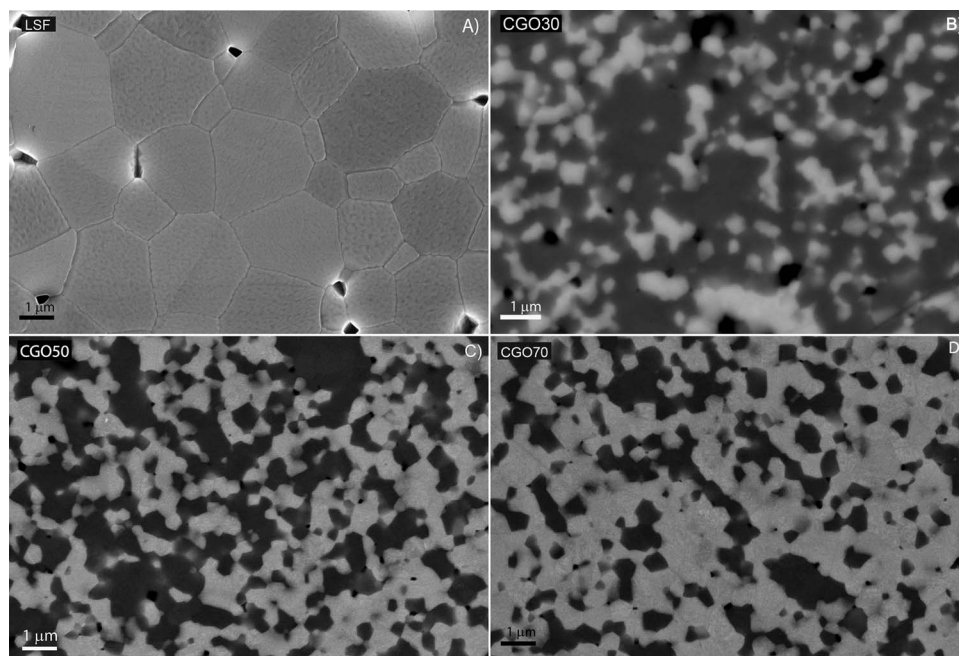
Figure 4. Scanning electron microscopy images of A) the pure LSF (secondary electrons), B) CGO30, C) CGO50, D) CGO70. B) C) D) images were recorded using back scatter detector for highlighting the compositional differences.

Oxygen exchange kinetics.—Figures 7A–7C shows the relaxation of the normalized conductivity and corresponding fitting curves (Eq. 5) after an instantaneous change of the oxygen pressure from 0.2 atm to 1.0 atm at 900°C, 750°C and 600°C. For the pure LSF 95% of the relaxation takes place in 5 min, 62 min and 30 h at 900°C, 750°C and 600°C, respectively. The addition of CGO to the LSF reduces the time of equilibration with the atmosphere, as is clearly seen in Figures 7A–7C, where all samples have a very similar size. The equilibration time decreases with an increased volume fraction of CGO and for the CGO70 it is 1 min, 13 min and 5 h at 900°C, 750°C and 600°C, respectively.

The decrease of the relaxation time by a factor of 5 reported in this study is smaller than the factor of 30 reported for $Sr_2Fe_{1.5}Mo_{0.5}O_6-Ce_{0.8}Sm_{0.2}O_{2-d}$ composites,[21,38] but is well in line with values reported for coated surface of dense LSCF bars with CSO, where a 6.5 times reduction of overall relaxation time was observed.[15] The decreased relaxation time points to the existence of synergistic effect between the LSF and CGO phases in the composite.

It should here be noted that the faster equilibration cannot be ascribed to just being an effect of that less oxygen is exchanged with increasing the CGO fraction. When the LSF fraction is decreased in the composite, the amount of exchanged oxygen on a pO_2 change is decreased but also the LSF surface area is decreased (both to the

same degree). Hence, if the CGO is totally inert in the oxygen surface exchange process the relaxation time should be unaltered (if the effect of tortuosity in oxygen incorporation path is neglected), as presented in Figure 1.

Fitting of the relaxation curves with Eq. 5 allows extraction of the D_{chem} and k_{ex} values. Figure 7D shows measured values for a CGO50 composite and different fitting curves assuming different sets of D_{chem} and k_{ex} values. The mismatch between measured and calculated curves shows that, when the k_{ex} value determined for LSF at the same measurement conditions (3.51×10^{-5} cm/s) is used for the composite (CGO50), the curve cannot be fitted by varying D_{chem} only (Figure 7D). The obvious conclusion is that not only D_{chem} is enhanced when introducing CGO, but also k_{ex} is enhanced in the composites compared to the pure LSF sample.

At 600°C and low pO_2 the rate of the equilibration process is completely controlled by the surface exchange process. This is illustrated in Figure 7E, showing an experimental curve for the LSF and CGO50 samples measured at 600°C, and $pO_{2 (end)}$ of 0.1 atm, where the best fit curves using both Eq. 1 and Eq. 5 are shown. The deviation between these two fitting curves is very small. Clearly, the data can be well fitted with only one parameter (k_{ex}), confirming the surface control. The direct comparison of the experimental data sets at these conditions, where oxygen exchange is completely oxygen exchange
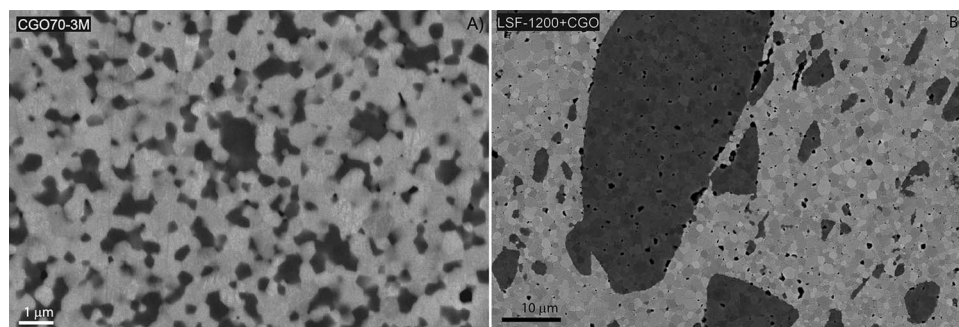
Figure 5. Scanning electron microscopy images of A) CGO70-3 M and B) LSF-1200+CGO using back scatter detector for highlighting the compositional differences.
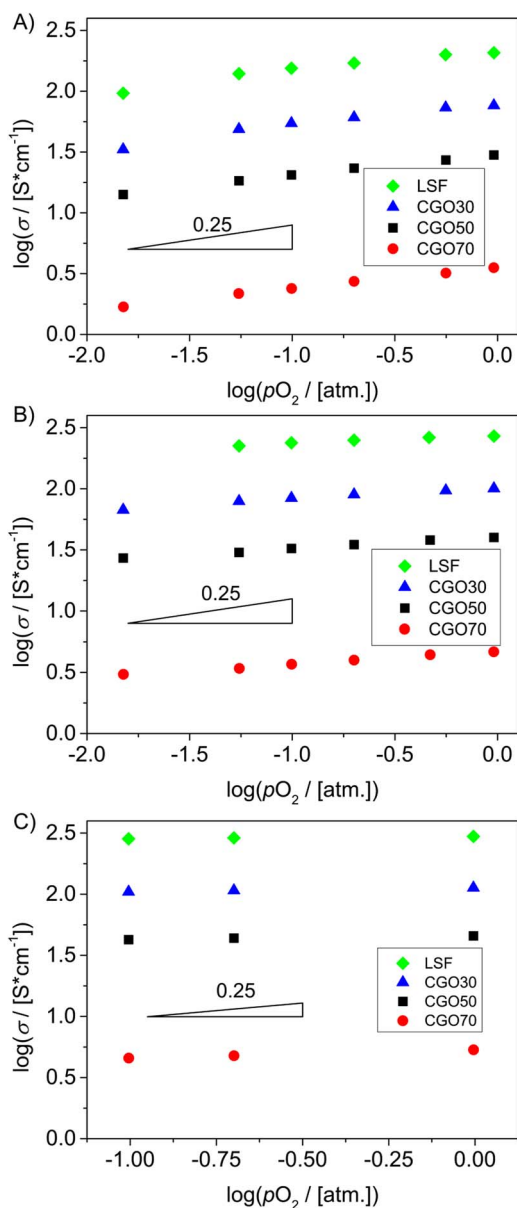
Figure 6. The total conductivity of the pure LSF and the LSF-CGO composites at different pO_2 A) at 900°C, B) at 750°C and C) at 600°C.

limited, again demonstrates that adding CGO enhances the oxygen exchange.

Figure 8 shows the D_{chem} values deduced from reduction steps at different pO_2 values and different temperatures for the LSF-CGO composites. D_{chem} decreases with temperature and is virtually independent on pO_2. Similar results have been reported for LSF in the literature.[9,10] For a slightly different LSF powder same D_{chem} of 1.8×10^{-5} cm²/s at 900°C has been reported by Søgaard et al.[11] D_{chem} increases with increasing volume fraction of CGO as expected, due to the high ionic conductivity of CGO compared to LSF. The effect of CGO addition is higher at lower temperatures, because of the increased difference between the ionic conductivities of CGO and LSF. The ionic conductivity of CGO and LSF are only a factor of three different at 900°C ($\sigma_{i(CGO)} = 0.155$ S/cm[54] and $\sigma_{i((La_{0.6}Sr_{0.4})_{0.99}FeO_{3-\delta})} = 0.049$ S/cm)[11] compared to at 750°C, where CGO is 20-times more conductive than LSF ($\sigma_{i(CGO)} = 0.069$ S/cm[54] and $\sigma_{i((La_{0.6}Sr_{0.4})_{0.99}FeO_{3-\delta})} = 0.003$ S/cm).[11] The theoretical values of D_{chem} for the dual-phase composites have been calculated by Eq. 7 and are shown in Figure 8. For the calculation of D_{chem} at 900°C a tortuosity τ_{IC} of 1 was as-

sumed. For the CGO30 sample a good agreement between calculated and measured D_{chem} values is observed. The measured D_{chem} values for the CGO50 sample were ~3 times higher than the calculated one and for the CGO70 were ~4-times higher. At 750°C the measured values correspond well to the calculated one with τ_{IC} of 1 for the CGO70 sample, whereas τ_{IC} of 2.5 and 20 were used for the CGO50 and CGO30 samples, respectively (Figure 8B) to match the measured and calculated D_{chem} values. At 600°C it was not possible to determine D_{chem} as oxygen transport in the samples is mainly limited by the oxygen surface exchange reaction.

Figure 9 shows k_{ex} taken from the reduction step and oxidation step as a function of the final pO_2 at different temperatures for all samples. Common to all obtained results is that k_{ex} increases with increased fraction of CGO and decreases with decreasing pO_2. The n value of $k_{ex} \propto pO_2{}^n$ is between 0.4 and 0.5 for pure LSF, CGO30 and CGO50 at 900°C. At 750°C the n value for the CGO50 sample is 0.4 and for the LSF and CGO30 samples it is 0.7. For the CGO70 sample a smaller pO_2 dependence of k_{ex} with $n = 0.3$ at both temperatures was observed. At 600°C only few measurements were done, due to a small and slow change of conductivity with pO_2, but the trend in Figure 9C shows that, the logarithmic pO_2 dependence of k_{ex} for the reduction steps was close to 1. For LSF a similar pO_2 dependence of k_{ex} was also reported in the literature.[7,9,11,26] Søgaard et al.[11] reported that the k_{ex} value at 900°C in air is 5.3×10^{-3} cm/s and that the pO_2 dependence of k_{ex} could be described as $k_{ex} = a \cdot pO_2{}^n$, where n was between 0.62 and 1.22 depending on the measurement temperature and ten Elshof et al.[10] reported a pO_2 dependence of k_{ex} of $0.75 < n < 0.83$ for a bulk LSF.

Involvement of the CGO surface.—In Figure 10 the measured k_{ex} values versus the fractions of CGO in the LSF-CGO composites at different temperatures and different pO_2 values are shown. The values presented in Figure 10 are obtained for two pO_2 steps from 0.05 atm to 0.1 atm and from 0.2 atm to 1.0 atm. The later pO_2 step is larger than for the results plotted in Figures 9A and 9B, but the same as was used for the relaxation measurement at 600°C (Figure 9C). A larger pO_2 step has been used at 600°C to get a significant change of conductivity. The highest k_{ex} was measured for the CGO70 composite at all temperatures and pO_2's and the smallest k_{ex} was measured for the pure LSF. The k_{ex} of the CGO70 for the pO_2 step from 0.2 to 1.0 atm at 750°C was 1.86×10^{-4} cm/s whereas for the pure LSF 3.51×10^{-5} cm/s was found. An even larger enhancement of k_{ex} for the dual-phase composites of $Sr_2Fe_{1.5}Mo_{0.5}O_3$-CSO at 750°C from 1.4×10^{-5} cm/s to 1.0×10^{-3} cm/s has recently been reported.[38]

Figure 10 clearly shows that k_{ex} increases with the CGO fraction, which indicates that the LSF surface is not the only surface where an oxygen exchange takes place, because in that case k_{ex} should remain the same with increased CGO fraction (Figure 1). Assuming that oxygen exchange may also occur on the CGO, the effective $k_{ex(cal)}$ was calculated according to Eq. 3, where the $k_{ex(CGO)}$ was selected as to give a best fit of Eq. 3 to the measured values for different temperatures and pO_2's. These best fit curves are the solid lines included in Figure 10 and the $k_{ex(CGO)}$ values are listed in Table II. For the $k_{ex(LSF)}$ the measured values of the pure LSF were used. k_{ex} increases in a roughly linear way with the increased volume fraction of CGO, which demonstrates that $k_{ex(CGO)}$ is significant, and that $k_{ex(CGO)} \geq k_{ex(LSF)}$. Rough estimations show that $k_{ex(CGO)}$ is pO_2 depended ($k_{ex(CGO)} \propto pO_2{}^1$) with the activation energy around 140 kJ/mol. The deduced values of $k_{ex(CGO)}$ are similar to the one reported for single phase pure $Ce_{0.85}Sm_{0.15}O_{2-d}$ investigated by the same method.[47]

To illustrate the range of the equivalent $k_{O(CGO)}$ values ($k_{O(CGO)} = k_{ex(CGO)}/\gamma_O$), they were calculated by using rough estimates of the thermodynamic enhancement factors (γ_O) for CGO calculated from the defect model reported in Ref. 50. Comparison to the measured k_O values by ^{18}O isotope diffusion profile is however very difficult, due to the large uncertainty on the γ_O for the CGO in this pO_2 and temperature interval. The uncertainty is estimated to be in one or even two orders of magnitude. The roughly estimated $k_{O(CGO)}$ values are lower than the both reported $k_{O(CGO)}$ values measured on a CGO-LSCF composite[40]
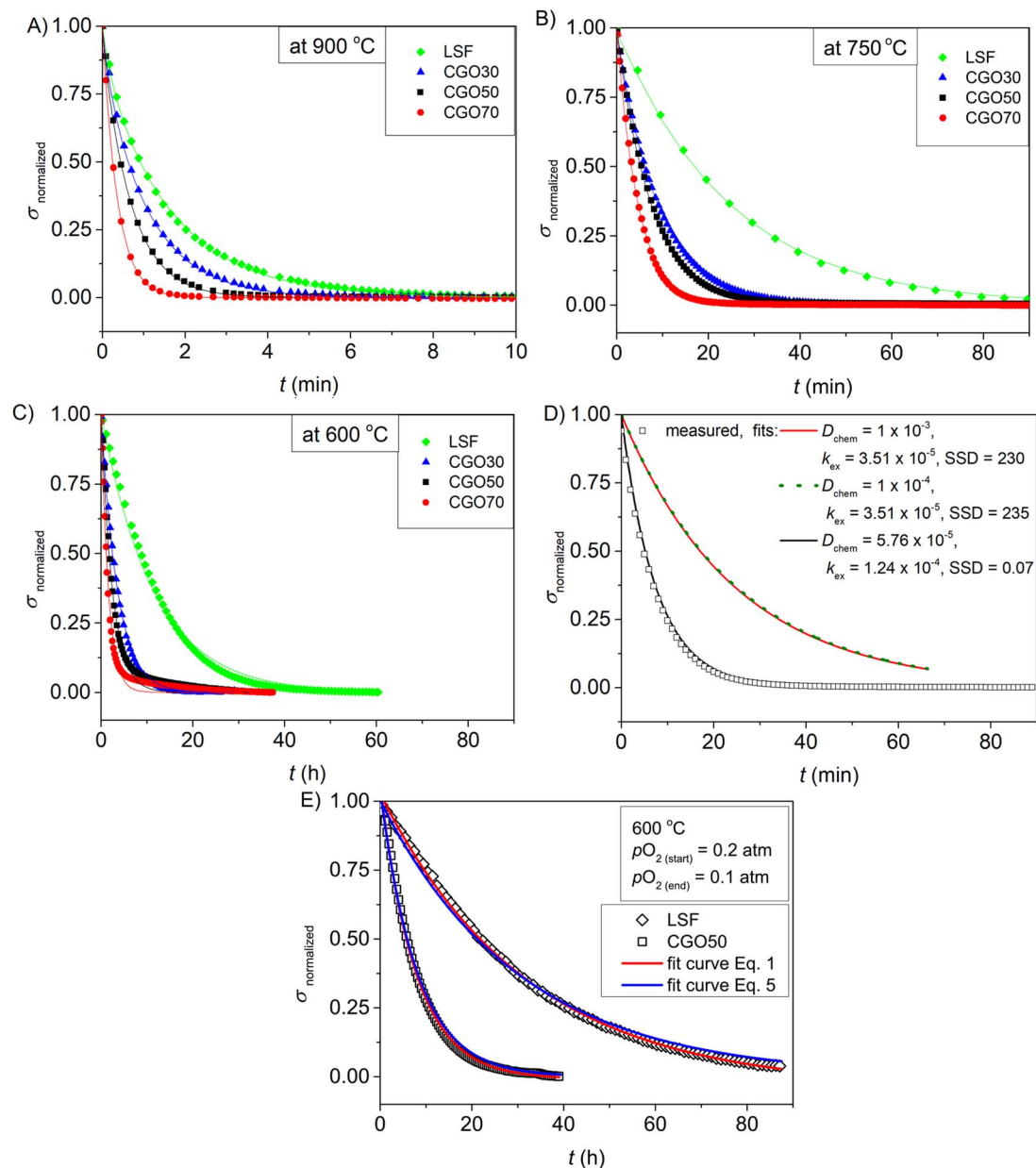
Figure 7. Electrical conductivity relaxation recorded for a pO_2 change from 0.2 atm to 1.0 atm at A) 900°C, B) 750°C and C) 600°C for the pure LSF and the LSF-CGO composites with corresponding fitting curves (lines). D) Measured ECR with different fitting curves for CGO50 at 750°C (SSD is the sum of squared deviations). E) ECR plots of the LSF and CGO50 samples measured at 600°C with corresponding calculated relaxation curves by Eq. 1 and Eq. 5.

Table II. Surface exchange coefficient of the CGO at different temperatures and pO_2's, obtained by fitting measured values by Eq. 3.

T (°C)	$k_{ex(CGO)}$ [cm s^{-1}] $pO_2 = 0.2$ atm	$k_{ex(CGO)}$ [cm s^{-1}] $pO_2 = 0.1$ atm	$k_{ex(CGO)}$ [cm s^{-1}] $pO_2 = 0.05$ atm	$k_{O(CGO)}$ [cm s^{-1}]	$K_{ex(LSF)}$ [cm s^{-1}] $pO_2 = 0.2$ atm
900	6.7×10^{-4}	5.1×10^{-4}	1.4×10^{-4}	6×10^{-9} ($\gamma_O \sim 115000$)	1.32×10^{-3}
750	1.1×10^{-4}	6.8×10^{-5}	3.4×10^{-5}	4×10^{-10} ($\gamma_O \sim 271000$)	3.51×10^{-5}
600	4.5×10^{-6}	/	/	9×10^{-12} ($\gamma_O \sim 512000$)	1.25×10^{-6}
850			8.5×10^{-4} $pO_2 = 10^{-3}$ atm, Ref. 47 *		
700				1.2×10^{-6}, CGO-LSCF, Isotope, Ref. 40	
700				1.1×10^{-8}, CGO, Isotope, Ref. 45	

*Ce$_{0.85}$Sm$_{0.15}$O$_{2-d}$.
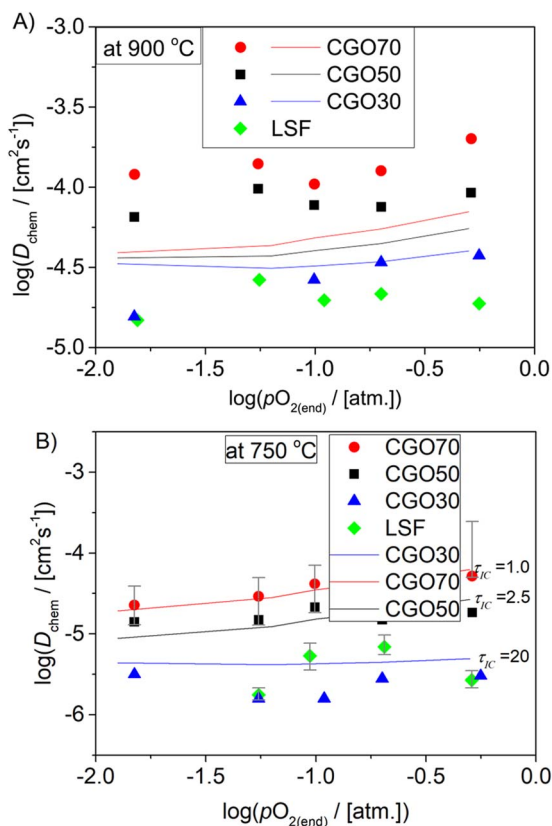
Figure 8. Logarithmic plot of chemical diffusion coefficient versus pO_2 for reduction relaxation measurements for the pure LSF and the composites at different temperatures: A) 900°C and B) 750°C. Symbols represent measured values and lines are calculated values by Eq. 7 at either fixed $\tau_{IC} = 1$ (900°C, A) or with τ_{IC} threated as a fitting parameter (750°C, B).

by oxygen isotope diffusion profiles, and the reported values on a pure CGO surface,[45] as listed in Table II.

In summary, it is thus possible to evaluate an apparent $k_{ex(CGO)}$ on the CGO phase in the composite from the measured relaxations and it is clear that the estimated values are significant and at low temperatures even faster than the LSF values. However, it is difficult to compare to the transport properties determined on CGO by more direct methods, such as isotope exchange measurements, due to high uncertainty on the thermodynamic enhancement factor.

Involvement of three phase boundaries.—Many studies on ionic conductor/MIEC composites have shown that the TPB (gas/ionic conductor/MIEC) plays a crucial rule in oxygen surface exchange process.[21,34,37,56] The contribution is mostly related to the concentration of oxygen vacancies, which is assumed to be higher at the TPB. Higher concentration can increase the surface exchange rate as stated in Fast oxygen exchange on grain boundaries section.

In Figure 11 the k_{ex} values for all here studied composites as a function of the measured TPB length are shown. The highest k_{ex} were measured for the composite with the shortest TPB lengths (2.1 µm/µm²) and more or less it seems that k_{ex} decreases with the TPB length. To exclude the effect of changed composition two composites with the same CGO/LSF ratio but different TPB lengths were compared. A slight decrease in the surface exchange coefficients was observed for the composites with longer TPB, with k_{ex} being lower at the CGO70-3 M sample than at the CGO70 sample. However, there is no obvious correlation between TPB length and k_{ex} in the range of here studied TPB lengths.

Surface impurities segregation.—The surface of the LSF-1200+CGO sample was characterized by TOF-SIMS, after exposing
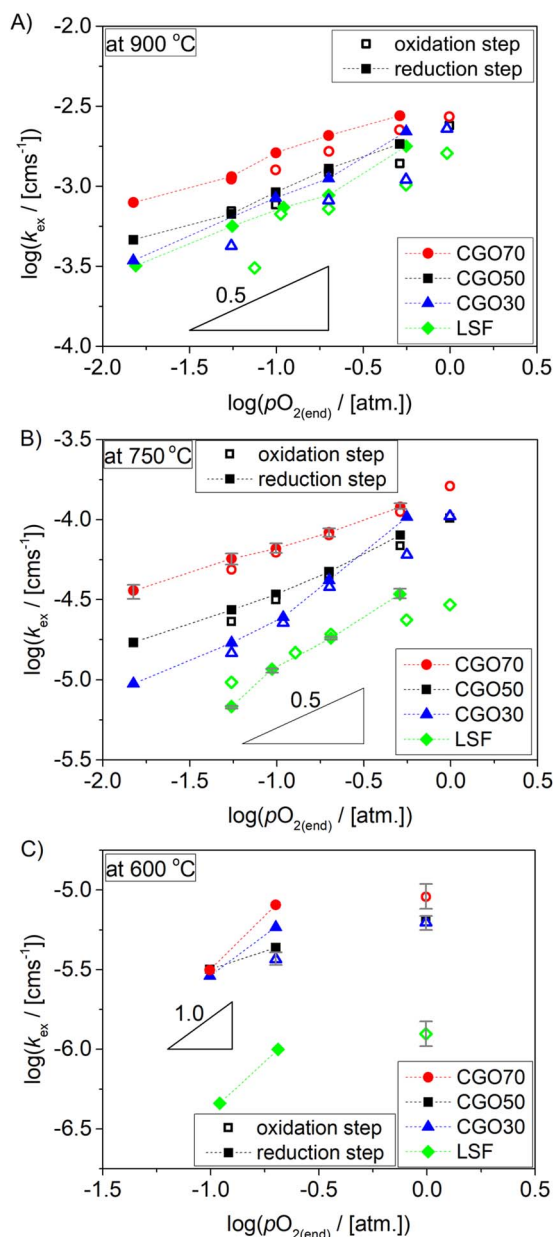
Figure 9. Logarithmic plot of the surface exchange coefficient versus pO_2 for the different composites and pure LSF A) at 900°C, B) at 750°C and C) at 600°C for the reduction steps (closed symbols) and the oxidation steps (open symbols).

it to similar conditions as the samples have experienced during the ECR. Results are shown in Figure 12. The LSF phase is clearly associated with a higher amount of impurities compared to the CGO phase. Specifically, for the surface of the LSF phase higher amounts of K, Na, Ca and Cr compared to the CGO surface were observed. One may thus speculate that, the presence of LSF in the dual-phase LSF-CGO composites cleans the CGO surface, which could allow the CGO to become more active in the oxygen surface exchange reaction.

The results reported here are in agreement with observed scavenging effect on a CGO-LSCF composite,[40] where none of the impurities (Na, Si, Ca) seen for the single phase CGO were evident when this material was a part of a composite. As reported by Druce et al.,[45] the presence of specific impurities; La-, Sr-, Fe- or Co-rich phases at the surface of CGO may also led to a drastic improvement of the oxygen exchange on CGO. This have been speculated by the formation of a SrCeO₃ perovskite phase on the surface of CGO that is able to
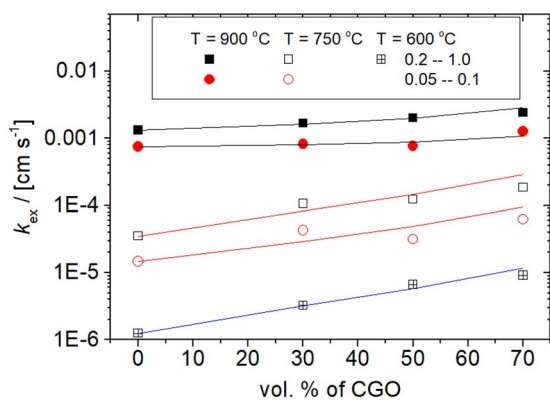
Figure 10. The average k_{ex} for composites at different temperatures for the pO_2 changes from 0.2 to 1.0 atm and from 0.05 to 0.1 atm (symbols). The calculated average $k_{ex(cal)}$ (Eq. 3) for the synergistic effect of the CGO and LSF phases (lines).
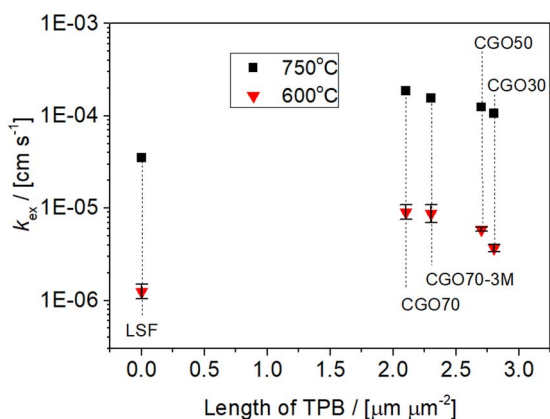
Figure 11. k_{ex} for a pO_2 change from 0.2 to 1.0 at 750°C and 600°C versus TPB length for all here studied composites.
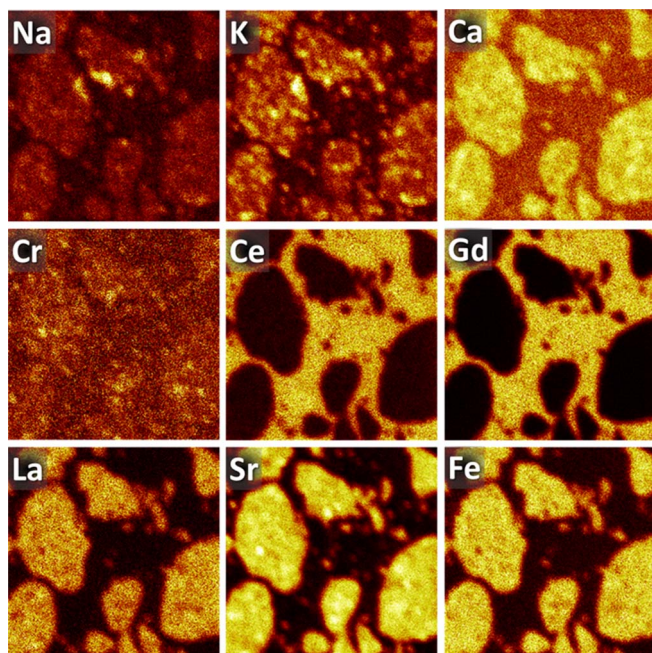
Figure 12. TOF-SIMS ion images (50×50 μm^2) normalized against the total ion image in order to remove possible instrument effects showing the microstructure of LSF-1200+CGO after ECR characterization.

incorporate a wide variety of elements with different charge and atomic radii on both A and B sites. This $SrCeO_3$ perovskite islands then can scavenge exchange impeding impurities from the CGO surface and it results in fast oxygen exchange on the ceria.[45]

In an opposite case, where a perovskite surface partially covered by ceria nanoparticles was studied, an enchantment of the exchange rate was also observed. LSCF bars decorated with CSO nanoparticles showed an increase in the surface exchange rate from 2.7×10^{-5} cm/s (bare LSCF) to 4.6×10^{-4} cm/s for the decorated sample as reported by Hong et al.[15] The improvement was ascribed to formation of a fast $LSCF/CGO/O_2$ interface. A large increase in surface exchange rate, up to 100 – times, was also observed for a $Sr_2Fe_{1.5}Mo_{0.5}O_6$ surface decorated with CSO nanoparticles.[38]

Discussion

In case of pure LSF the surface exchange reaction at high pO_2's ($10^{-3} < pO_2 < 1$ atm), by assuming the involvement of oxygen vacancies in the oxygen surface exchange process,[10] will be strongly depended on the mobility and/or concentration of oxygen vacancies, while for pure CGO the oxygen exchange will be presumably limited by the electronic conductivity.[50] From the results reported here it is seen that combining LSF and CGO into a composite is beneficial and that the surface exchange rate is enhanced with increasing the fraction of CGO in the composite. The enhancement is larger at lower temperatures. The enhanced surface exchange coefficient with increasing amount of CGO indicates that the CGO is involved directly in the oxygen surface exchange reaction. In principle, as also discussed in Fast oxygen exchange on grain boundaries section, the increasing exchange rate could be due to the introduction of fast BG/TPB upon the introduction of CGO. However, as the enhancement does not scale with the observed TPB length, it does not seem the dominant effect in this system.

The observed CGO involvement in the oxygen surface exchange reaction could be speculated to occur via different routes, for example;

i) The CGO is involved in surface exchange reaction or into one of the oxygen exchange steps. For example; reduced oxygen species formed on the LSF surface could spill over to the CGO surface. In this case the CGO surface is active in the subsequent dissociation of partly reduced oxygen species to the atomic species and/or their incorporation. This will also act as removal of intermediate oxygen species formed on the LSF, which would otherwise impede the incorporation reaction. This agrees with the here reported experimental result that both CGO and LSF surfaces are active in the oxygen surface exchange reaction.

ii) One phase scavenges impurities from other, thereby making one of the phases much faster for oxygen exchange than when this phase is present alone. Indeed, here we found larger amount of alkali impurities on the LSF than on the CGO. Hence, it could be, that a cleaning of the CGO surface takes place via the presence of LSF, making the oxygen exchange on CGO much faster than when considering single phase CGO samples. This would be consistent with the observations here and with results on CGO and LSCF-CGO composites reported by Druce et al.[40,45] Additionally, the results reported by Gopal and Haile[47] on k_{ex} of Sm doped CeO_2 surface studied as a single phase material also show that in some cases the oxygen surface exchange reaction at high pO_2 on doped ceria can be fast.

Although further studies are needed, e. g. replacing CGO with better or worse ionic or electronic conductors, to verify the influence of conductivities, we find that both routes involving spillover of oxygen species from one phase to the other and enhanced exchange on CGO itself due to impurity scavenging in LSF are supported by the presented data and both are likely possible. It should also be pointed out that these two mechanisms are not mutually exclusive and can act simultaneously.

Further, the pO_2 dependence of k_{ex}, which was observed to vary with the CGO fraction and the temperature, can point out different aspects of the mechanism of the oxygen exchange. Different *rds* can be assumed depending on the observed exponent n ($k_{ex} \propto pO_2{}^n$): i) $n \approx 1$ indicates that molecular oxygen participates in the *rds*, ii) $n \approx 0.5$ indicates the involvement of atomic oxygen species in the *rds* and iii) $n \approx 0.25$ would indicate the involvement of electron transfer or oxygen incorporation in the *rds*.[7,18]

For the LSF-CGO composites presented in this study the n ($k_{ex} \propto pO_2{}^n$) was between 0.3 and 1.0 and varied with the composition and temperature. The broad range of observed pO_2 dependences disenables a decisive conclusion about the *rds* of the oxygen surface exchange reaction. However, two trends are clear:

i) Firstly, that the *rds* depends on the temperature. Higher n values ($k_{ex} \propto pO_2{}^1$) are observed at lower temperature, which point toward the involvement of oxygen molecules in the *rds*, as also found by ten Elshof et al.[10] At low temperature, it is expected that the adsorption/desorption reaction will be slower than at higher temperatures. Additionally, other strongly adsorbed molecules (e.g. CO_2) or intermediate oxygen species can contribute to even slower adsorption/desorption reaction of oxygen through covering of active sites. While, at high temperature overall pO_2 dependence of k_{ex} points in the direction of atomic oxygen species being involved in the *rds*.

ii) Secondly, if oxygen vacancies are involved in the *rds* the pO_2 dependence of k_{ex} would be influenced by the composition of the composite. The vacancies in LSF respond differently to the change of pO_2 and temperature than vacancies in CGO. The pO_2 dependence of the oxygen vacancy concentration in the CGO for the studied conditions is close to zero ($[V_O^{\bullet\bullet}] \propto pO_2{}^0$) and for LSF is close to $-1/2$ ($[V_O^{\bullet\bullet}] \propto pO_2{}^{-1/2}$).[11] In this case, it is expected that an increase of the CGO fraction in the composite will, for a vacancy dependent *rds*, result in numerically smaller n-values (such a trend was observed at 900°C and 750°C).

The theoretical values of D_{chem} for the dual-phase composites calculated by Eq. 7 were compared with the measured D_{chem}. At high temperature (900°C) by assuming tortuosity τ_{IC} of 1 small discrepancy was observed between the measured and the calculated D_{chem}. The measured D_{chem} values for the CGO50 sample were ∼3 times higher than the calculated one, and for the CGO70 were ∼4-times higher, but for the CGO30 sample a good agreement between the calculated and the measured values was observed. This could reflect an additional contribution of the oxide ions diffusion along grain boundaries in the dual-phase composites. It is clear that at high temperatures (900°C), where the ionic conductivity of CGO and LSF are more similar, the effect of a tortuous path of the ionic transport will be lower compared to at low temperatures (750°C), where the ionic conductivity of LSF is significantly smaller than that of CGO. At 750°C the measured values for the CGO70 sample behaves as expected from the materials properties and increasing the LSF fraction leads to large deviations from the values obtained by volume weighting average, which is interpreted as a tortuosity effect.

Conclusions

Based on electrical conductivity relaxation measurements of the LSF-CGO dual-phase composites with different phase ratios and morphologies it is concluded that; (i) the bulk diffusion properties of the composites behave as expected for the material properties with relatively large contribution from tortuosity effect at low temperatures, (ii) the CGO surface is involved in the oxygen surface exchange reaction, (iii) increased fractions of CGO in a dual-phase composite (from 30% to 70%) enhances the oxygen surface exchange reaction and, (iv) the enhancement of k_{ex} does not scale with the TPB length. Considering all experimental data it is further suggested that the *rds* is temperature and composition dependent. The involvement of CGO in the oxygen exchange can be through the spillover of oxygen ions, partly

reduced oxygen species, from LSF to CGO, where they dissociate and/or incorporate. An alternative effect could be that the LSF scavenges impurities from CGO and thereby activates the CGO surface for the oxygen surface exchange reaction. Both proposed mechanism could account for the observations.

ORCID

Simona Ovtar https://orcid.org/0000-0003-4588-2679

References

1. S. Cheng et al., *ACS Appl. Mater. Interfaces*, **8**, 4548 (2016).
2. R. J. Gorte, J. M. Vohs, and J. M. Prausnitz, Editor. *Annu. Rev. Chem. Biomol. Eng.*, **2**, 9 (2011).
3. Z. P. Shao and S. M. Haile, *Nature*, **431**, 170 (2004).
4. J. H. Joo, G. S. Park, C.-Y. Yoo, and J. H. Yu, *Solid State Ionics*, **253**, 64 (2013).
5. S. B. Adler, *Solid State Ionics*, **111**, 125 (1998).
6. J. Hayd, L. Dieterle, U. Guntow, D. Gerthsen, and E. Ivers-Tiffee, *J. Power Sources*, **196**, 7263 (2011).
7. M. Mosleh, M. Sogaard, and P. V. Hendriksen, *J. Electrochem. Soc.*, **156**, B441 (2009).
8. M. V Patrakeev et al., *J. Solid State Chem.*, **172**, 219 (2003).
9. W. Preis, E. Bucher, and W. Sitte, *Solid State Ionics*, **175**, 393 (2004).
10. J. E. TenElshof, M. H. R. Lankhorst, and H. J. M. Bouwmeester, *J. Electrochem. Soc.*, **144**, 1060 (1997).
11. M. Sogaard, P. V. Hendriksen, and M. Mogensen, *J. Solid State Chem.*, **180**, 1489 (2007).
12. I. Waernhus, T. Grande, and K. Wiik, *Top. Catal.*, **54**, 1009 (2011).
13. W. Zhang, *thesis*, *Department of Energy Conversion and Storage*, Technical University of Denmark (2012).
14. B. T. Dalslet, M. Sogaard, and P. V. Hendriksen, *Solid State Ionics*, **180**, 1050 (2009).
15. T. Hong, L. Zhang, F. Chen, and C. Xia, *J. Power Sources*, **218**, 254 (2012).
16. T. Ishigaki, S. Yamauchi, K. Kishio, J. Mizusaki, and K. Fueki, *J. Solid State Chem.*, **73**, 179 (1988).
17. E. N. Armstrong, K. L. Duncan, and E. D. Wachsman, *Phys. Chem. Chem. Phys.*, **15**, 2298 (2013).
18. R. Merkle and J. Maier, *Phys. Chem. Chem. Phys.*, **4**, 4140 (2002).
19. S. B. Adler, X. Y. Chen, and J. R. Wilson, *J. Catal.*, **245**, 91 (2007).
20. R. Merkle and J. Maier, *Top. Catal.*, **38**, 141 (2006).
21. Y. Wang, B. Hu, Z. Zhu, H. J. M. Bouwmeester, and C. Xia, *J. Mater. Chem. A*, **2**, 136 (2014).
22. L. Wang, R. Merkle, Y. A. Mastrikov, E. A. Kotomin, and J. Maier, *J. Mater. Res.*, **27**, 2000 (2012).
23. J. Fleig, R. Merkle, and J. Maier, *Phys. Chem. Chem. Phys.*, **9**, 2713 (2007).
24. I. Yasuda and M. Hishinuma, *Solid State Ionics*, **80**, 141 (1995).
25. J. E. tenElshof, M. H. R. Lankhorst, and H. J. M. Bouwmeester, *Solid State Ionics*, **99**, 15 (1997).
26. M. Sogaard, A. Bieberle-Huetter, P. V. Hendriksen, M. Mogensen, and H. L. Tuller, *J. Electroceramics*, **27**, 134 (2011).
27. L. M. van der Haar, M. W. den Otter, M. Morskate, H. J. M. Bouwmeester, and H. Verweij, *J. Electrochem. Soc.*, **149**, J41 (2002).
28. R. A. De Souza and J. A. Kilner, *Solid State Ionics*, **126**, 153 (1999).
29. R. Merkle, J. Maier, and H. J. M. Bouwmeester, *Angew. Chemie-International Ed.*, **43**, 5069 (2004).
30. J. A. Kilner, R. A. DeSouza, and I. C. Fullarton, *Solid State Ionics*, **86–8**, 703 (1996).
31. Y. Wang, L. Zhang, and C. Xia, *Int. J. Hydrogen Energy*, **37**, 2182 (2012).
32. A. Banerjee and O. Deutschmann, *J. Catal.*, **346**, 30 (2017).
33. Y. Ji, J. A. Kilner, and M. F. Carolan, *J. Eur. Ceram. Soc.*, **24**, 3613 (2004).
34. S. P. Jiang and W. Wang, *J. Electrochem. Soc.*, **152**, A1398 (2005).
35. X. Xu, Z. Jiang, X. Fan, and C. Xia, *Solid State Ionics*, **177**, 2113 (2006).
36. M. H. R. Lankhorst, H. J. M. Bouwmeester, and H. Verweij, *Phys. Rev. Lett.*, **77**, 2989 (1996).
37. B. Hu, Y. Wang, and C. Xia, *J. Power Sources*, **269**, 180 (2014).
38. L. Zhang et al., *Electrochem. commun.*, **13**, 711 (2011).
39. R.-W. You, J. Ouyang, Y.-P. Fu, S.-H. Hu, and K.-W. Tay, *Ceram. Int.*, **39**, 8411 (2013).
40. J. Druce, H. Téllez, T. Ishihara, and J. A. Kilner, *Faraday Discuss.*, **182**, 271 (2015).
41. F. Bidrawn, G. Kim, N. Aramrueang, J. M. Vohs, and R. J. Gorte, *J. Power Sources*, **195**, 720 (2010).

42. S. Saher et al., *J. Mater. Chem. A*, **5**, 4991 (2017).
43. P. Manning, *Solid State Ionics*, **93**, 125 (1996).
44. J. D. Sirman and J. A. Kilner, *J. Electrochem. Soc.*, **143**, L229 (1996).
45. J. Druce and J. A. Kilner, *J. Electrochem. Soc.*, **161**, F99 (2014).
46. G. J. Ia O' and Y. Shao-Horn, *J. Electrochem. Soc.*, **156**, B816 (2009).
47. C. B. Gopal and S. M. Haile, *J. Mater. Chem. A*, **2**, 2405 (2014).
48. Y. Wang, Y. Wang, and C. Xia, *J. Electrochem. Soc.*, **159**, F570 (2012).
49. E. Navickas et al., *Phys. Chem. Chem. Phys.*, **17**, 7659 (2015).
50. C. Chatzichristodoulou and P. V Hendriksen, *Phys. Chem. Chem. Phys.*, **13**, 21558 (2011).
51. O. F. Lohne et al., *J. Electrochem. Soc.*, **161**, F176 (2014).
52. P. Hjalmarsson, M. Sogaard, and M. Mogensen, *Solid State Ionics*, **180**, 1290 (2009).
53. J. E. Mortensen, M. Sogaard, and T. Jacobsen, *J. Electrochem. Soc.*, **161**, F161 (2014).
54. B. Dalslet et al., *J. Solid State Electrochem.*, **10**, 547 (2006).
55. S. Ovtar et al., *J. Memb. Sci.*, **523**, 576 (2017).
56. Y. Ji, J. A. Kilner, and M. F. Carolan, *Solid State Ionics*, **176**, 937 (2005).